A Comparison of Modeling Methods for Predicting the Elastic-Plastic Response of Additively Manufactured Honeycomb Structures

Raghav Sharma[1], Thao Le[1], Jiaxu Song[1], Ethaniel Harms[1], Daniel Sowa[1], Alex Grishin[2], Dhruv Bhate[1]

[1]Arizona State University, Mesa, AZ 85212
[2]Phoenix Analysis & Design Technologies, Inc., Tempe, AZ 85284

Abstract

Valid and accurate models describing the mechanical behavior of additively manufactured cellular materials are crucial to enabling their implementation in critical-to-function parts. Broadly speaking, the modeling approaches commonly used in the literature fall into three categories. Each of these differs in the level of discretization at which the cellular behavior is modeled: at the level of each material point, at the level of the unit cell or at the level of a connecting member that constitutes a unit cell. Each of these three approaches relies on different characterization techniques and the way in which the resulting data is leveraged in the development of the model. In this work, we critically examine all three modeling approaches using FEA and compare their accuracy in the prediction of the elastic and plastic behavior of experimentally characterized hexagonal honeycomb structures made with Fused Deposition Modeling, and discuss the pros and cons of each method.

Introduction

Modeling, for the purposes of this paper, refers to the methods of *prediction* of the behavior of cellular materials. Modeling is important for at least two reasons: first, it enables the translation of predictability from a lower level of complexity (like a tensile test specimen) to the application at hand (such as a rotating fan blade). This is a key step in validation since not everything can be tested in every environment possible. Modeling also serves another purpose - it drives optimization and allows us to improve performance. Models allow us to gain insight into the design variables that matter and enable the evaluation of multiple design options in search of the optimal one.

For a model to be of practical value, it needs two key ingredients working together. The first of these is a mathematical description that relates behavior to design and material parameters (this could be analytical and/or leverage computational tools such as Finite Element Analysis - FEA). Secondly, the model needs a quantified material representation that can be implemented into the mathematical description. In this paper, we focus on the different ways cellular materials can be represented for use in FEA software – in other words, we investigate how the material properties can be determined and represented for accurate results.

A Review of Approaches

Material modeling approaches for cellular materials fall into three different categories, depending on the level of discretization at which the property is modeled. Arranging these in order of the scale at which material behavior is represented, these models can operate at the level of each material point (bulk property models), at the level of the connecting member (member models) or

finally, at the level of the cell (homogenization models). In the following sections, we deal with each of the three in turn, but in a slightly different order to enable meaningful comparisons.

1. Bulk Property

The most straightforward approach in modeling cellular materials is to use bulk material properties to represent what is happening to the material at the cellular level. This approach does away with the need for any cellular level characterization and in so doing, does not have to account for size effects or other experimental artifacts that are specific to cellular materials. ASTM or ISO standards can be leveraged to develop databases of material behavior and this allows for a proper statistical basis to be established. However, the assumption that the connecting struts/walls in a cellular structure behave the same way the bulk material does can particularly be erroneous for AM processes that can introduce significant size-specific behavior and large anisotropy. There are two reasons for this – the first has to do with the process dependence inherent to most AM processes, the second has to do with the geometry related variations specific to cellular materials themselves.

Most AM processes have a strong orientation dependence to their mechanical properties, with the build direction being typically the weaker, in comparison to the in-plane properties. These differences are strongly process dependent, with parts made with Fused Deposition Modeling (FDM) processes being strongly anisotropic on one end, and Electron Beam Melting parts being less so at the other end of the spectrum. However, anisotropy can be represented in orthotropic material models to mitigate the impact of these differences. What is harder to represent is the dependence of the properties on the *meso- and/or microstructure*, which in turn often has strong dependence on the process settings used to realize that part. In the example shown in Figure 1, for the FDM process, four ASTM D638 standard specimens were manufactured with the identical geometry, but varying process parameters – in this case, the number of contours and rasters in the part was varied. The resulting load-displacement curves are significantly different to each other, implying process dependent elastic moduli and failure stresses.
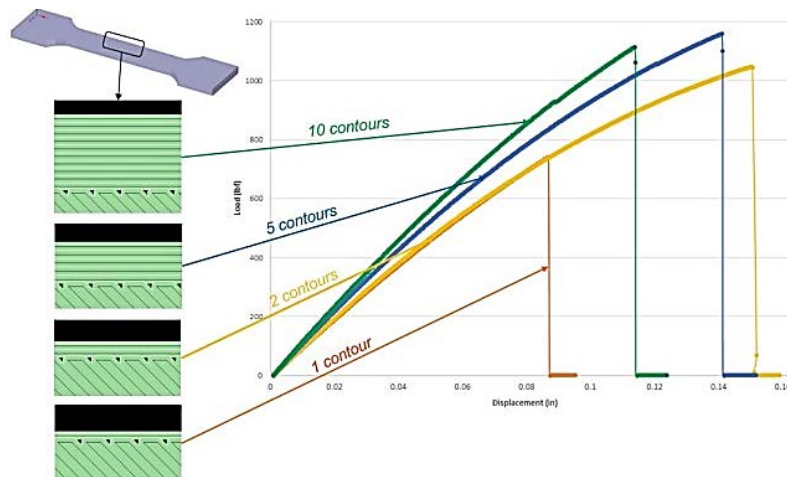
Figure 1. Effect of processing parameters (number of contours) on tensile load-displacement for the Fused Deposition Modeling process

The reason process dependence matters particularly for cellular materials comes down to their typically fine features. For a thin strut or wall, the additive process may only pass through a

given feature a few times in each layer. In many cases, 1 or 2 contours are all that is needed to create the feature at that layer. As shown in Figure 2 for thin walls made with laser powder bed fusion (LPBF), as the thickness of the feature increases, additional passes are needed, which in turn can change the microstructure and mechanical behavior of the cellular material as an aggregate.
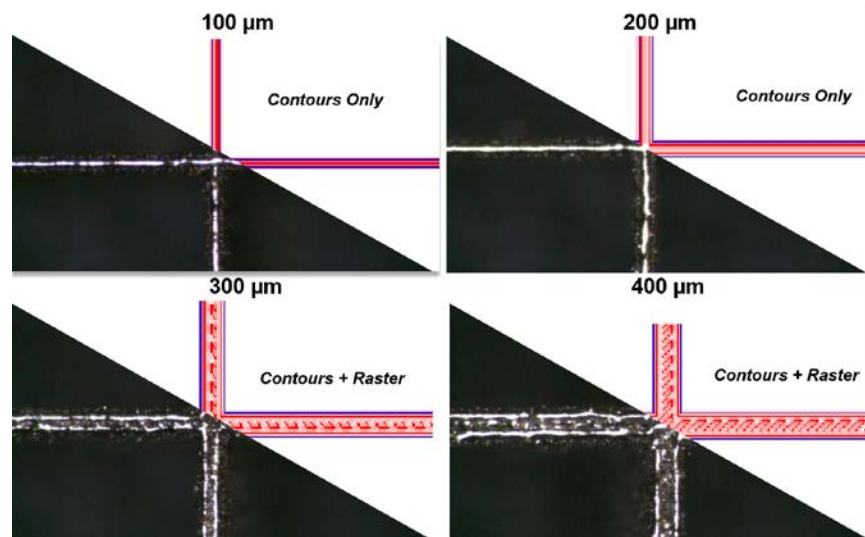
Figure 2. As feature thickness increases, more passes of the laser are needed, resulting in modifications to structure (shown here for the Laser Powder Bed Fusion process)

Most additively manufactured cellular materials tend to have feature dimensions on the order of tens to hundreds of microns. Most of the processes are themselves capable of printing parts on the order of hundreds of millimeters. This combination of resolving fine features in relatively large parts is one of the attractive aspects of AM technologies, but does introduce a challenge from a modeling perspective. Consider the honeycomb structure in Figure 3, for example, manufactured on a production grade FDM system (the Stratasys Fortus 400mc) [1]. Measurements of the wall thicknesses show an average error between measured and designed thicknesses of 100 µm, which is within the machine specifications and ordinarily is not noteworthy. However, this minor variation amounts to a 7% error in the true thickness of the honeycomb walls as designed. In honeycombs, which are bending-dominated for thin wall structures, the effective modulus of the structure scales by the cube of the thickness, so this would be a very large source of error in modeling the honeycomb. For stretch-dominated structures such as lattices, modulus scales linearly, so this would still amount to a significant error. Therefore, dimensional errors that are within specifications at the level of bulk structures including typical ASTM/ISO test specimens, are significant first-order errors when the dimensions get as small as they do. It is for this reason that models that exclude these effects, as bulk property models do, are unlikely to be good predictors of behavior, unless corrections are made to the model to account for them.

Dimensions are only one of the sources of imperfection that bulk property models do not take into consideration. The others include surface roughness, waviness, defects like pores and cross-section variations by orientation, all of which are discussed for the LPBF process in a paper by Liu et al. [2]. Some researchers use bulk property assumptions but then develop correction

factors to get good agreement between model and experiment, as demonstrated for Selective Laser Sintering (SLS) process by Neff et al. [3] and the LPBF process by Smith et al. [4].

(a)   (b)

(c)
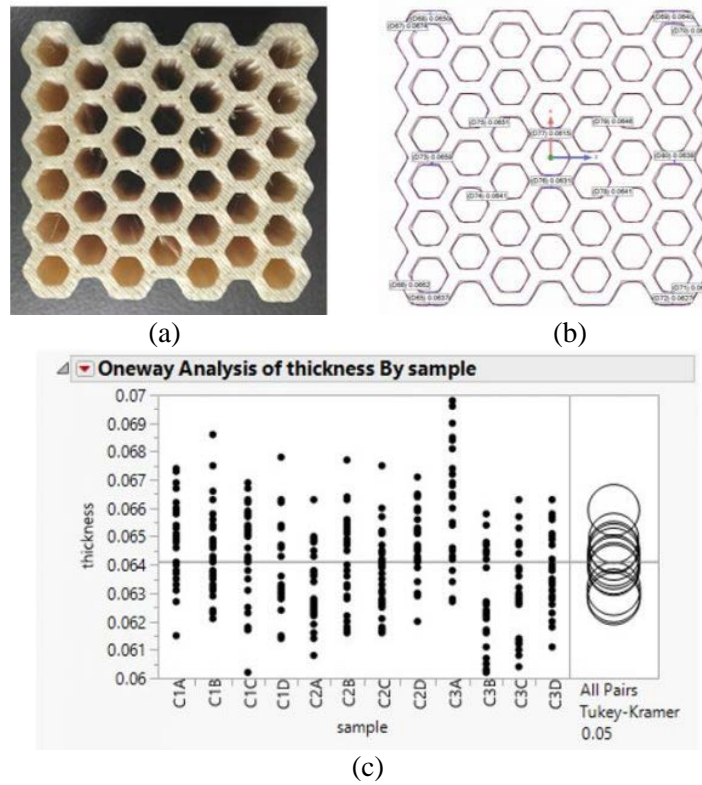
Figure 3. (a) A honeycomb sample, (b) optical scan image using blue light scanning and (c) 12-sample data showing a mean of 1.625mm against a designed value of 1.524mm – a 7% error in thickness, adapted from Le et al. [1]

2. Homogenization

Homogenization involves estimation of an *effective property* of the cellular structure without explicit regard to the cellular geometry itself. These properties are determined experimentally through characterization of cellular materials, and in that sense represent an improvement over the bulk property method. Another advantage inherent to homogenization is that this approach has significantly lower computational expense associated with its implementation in simulation software since the cellular structure is not explicitly modeled in the computational environment but instead replaced with a solid structure that has effective properties, as shown in Figure 4. Additionally, it is relatively straightforward to develop a model by fitting a power law to experimental data as discussed before and shown in the equation below, relating the effective modulus E^* to the bulk material property E_s and their respective densities (ρ and ρ_s), by solving for the constants C and n. Similar equations can be developed and fitted to the observed data for other material parameters of interest.

$$E^* = C\, E_s \left(\frac{\rho}{\rho_s}\right)^n \qquad\qquad (1)$$
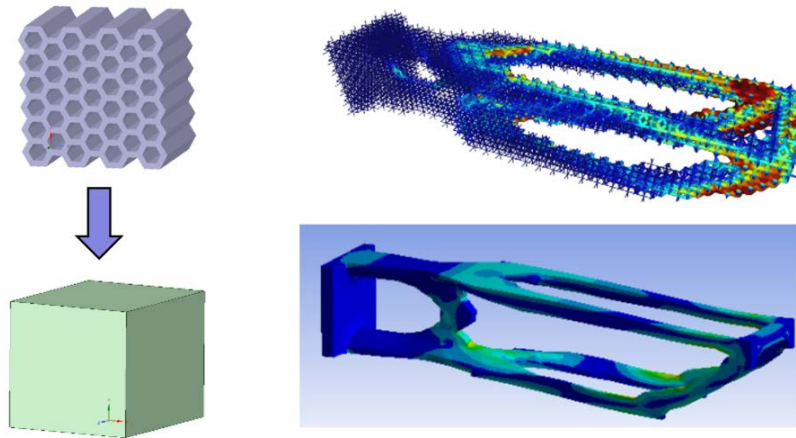
Figure 4. (left) Homogenization enables the replacement of a cellular material with a solid of effective properties, (right) which can greatly reduce computational expense when simulating engineering structures

The homogenization approach has been used by several researchers in the literature [5]–[8] and while it has the advantages mentioned above, it also has some difficulties in being used as a reliable material model in analysis & simulation that need to be taken into consideration. An immediate limitation of homogenization is that it is dependent on the cell shape – each shape needs to be individually characterized and relationships developed. Further, this needs to be done at different volume fractions, otherwise the model is limited to one specific size for a given shape. This increases the experimental effort required significantly, in comparison with the other approaches discussed in this section. A second, more serious limitation arises from the fact that for a given shape, there are two ways to modulate the volume fraction – change the size of the cell, or change the thickness of the struts or walls that make up the cell. It has been shown that these two ways of modulating the volume fraction do not result in similar calculations of modulus and other properties – in other words, homogenization models based on relative density alone are prone to error. Finally, it is not clear if homogenization models can predict well the behavior of structures with non-uniform cell size since transitions between different relative densities can introduce shapes that do not conform to the shape assumptions in the model. Nonlinear behavior, damage and fracture are also harder to model since these are so geometry dependent, transient phenomena.

All these limitations when taken together, place serious constraints on homogenization models for cellular materials. While they are likely to serve well when the shape and size of the cellular material is fixed and known, they do not lend themselves well to the spirit of AM and the design freedom it enables.

3. Member Modeling

The two above approaches seek to represent cellular material behavior at two extreme ends: the bulk property approach seeks to establish a point-wise material representation whereas the homogenization approach seeks to do so at the level of the unit cell. The third approach, which we may term member modeling, involves describing behavior at a level in-between, viz. the connecting member or element that networks to constitute the cellular structure. This is done by identifying an elemental member that constitutes the cellular material and designing and testing a specimen that embodies that member, as shown in Figure 5.
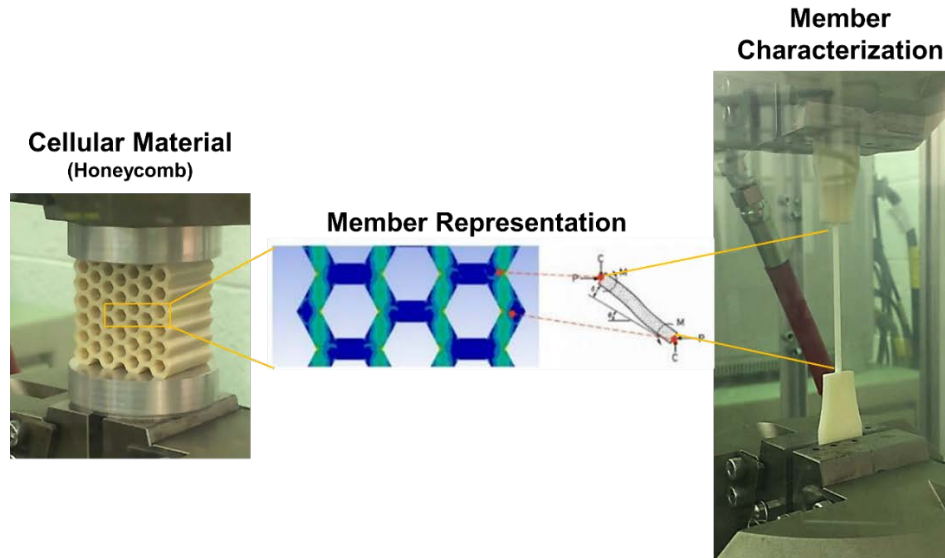
Figure 5. Member modeling involves identifying the key member contributing to the deformation and characterizing it

The basic notion of the member modeling method (though with different terminology such as micro-strut for lattice materials) has been used by several researchers with mixed results [1], [9]–[13]. The advantage of this approach is that if we are able to accurately describe behavior at the level of a connecting member, it enables a truly shape independent model [1]. Additionally, more insight can potentially be gained by studying an individual member than by characterizing cellular materials due to the latter's sensitivity to a range of experimental artifacts such as size effects and strain rate sensitivity – both of which can be better controlled and studied at the level of an individual member [12].

The member modeling approach, while promising, has its own set of challenges: it requires experimental characterization at the level of micro-struts or thin walls, which can prove to be difficult to accomplish due to the very fine feature sizes involved. However, this challenge is not insurmountable with proper experimental procedures and the right specimen design. The second challenge is regarding the accuracy of the representation – how well can individual struts and walls describe what is happening in a complex cellular structure with different orientations and local thermal conditions that may be different from the struts is something that needs significant validation that may be specific to each process and material.

Characterization

Each of the three modeling methods mentioned previously relies on material properties from two sources – either this emerges from characterization of the bulk property by ASTM standard test procedures, or through testing of miniature specimens created to represent the member. In this section, we discuss the origins of these properties for both sources, prior to implementing them in the models for predicting behavior. We begin though by establishing our experimental dataset that will form the reference for comparing each modeling method against. This data comes from prior work [1], the key aspects of which are recounted here.

1. Honeycomb Compression

In prior work [1], an approach for extracting the elastic modulus of a honeycomb independent of its shape and size was proposed. As part of that work, square, hexagonal and triangular honeycombs of different sizes were tested under compression on an INSTRON 8801 tester. These honeycombs were manufactured with the Fused Deposition Modeling process on a Stratasys Fortus 400mc machine with ABS material. Details of the manufacturing and testing process, and the honeycomb design can be found in the cited reference. The primary result of interest is the compression load-displacement response shown in Figure 6. The deformation followed a pattern shown in Figure 7. While Figure 6 is one representative sample, it adequately captures the elastic-plastic behavior we are trying to model and predict and as such is used as the comparative baseline in this study.
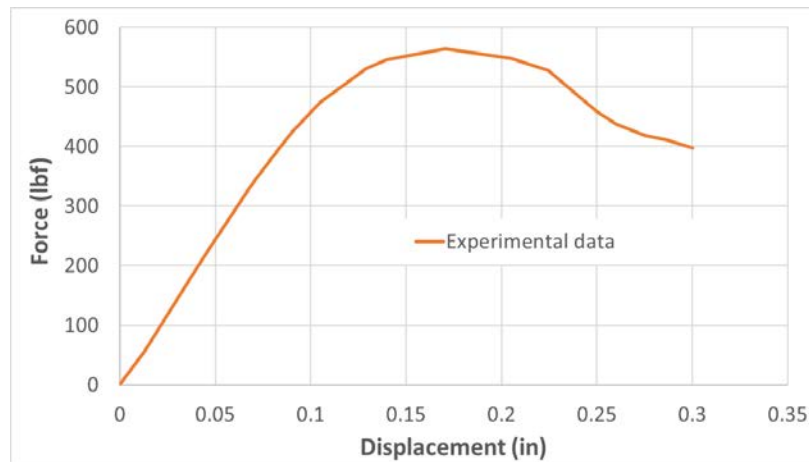
Figure 6. Load-displacement response under compression associated with the honeycomb specimen shown in Figure 7
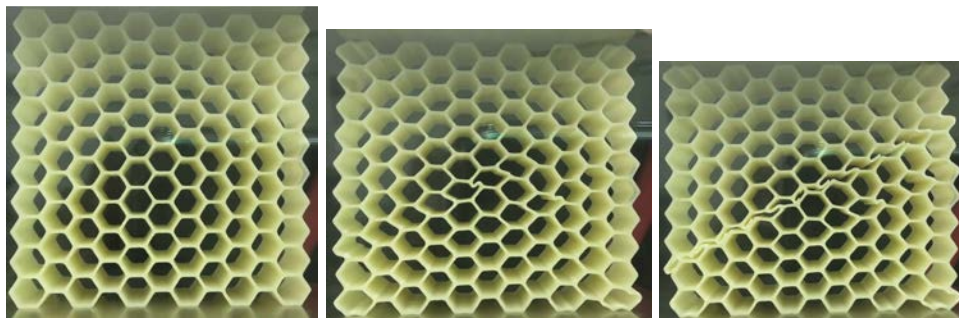
Figure 7. Compression of a hexagonal honeycomb – images not to relative scale (details in [1])

2. Bulk Properties

Bulk properties were obtained from the supplier datasheet [14] for the ABS-M30 material and the Fused Deposition Modeling (FDM) process that was used to manufacture the honeycombs used in this study. Since the datasheet specifies properties based on ASTM D638 standard specimen designs built in two different orientations, the orientation that best aligned with the honeycomb construction was selected (XZ axis). Since we are interested in the elastic-plastic response, the tensile modulus and the yield strength were obtained from the datasheet, as 320,000 psi and 4,550 psi, respectively. Poisson's ratio is not specified in the datasheet, so a value of 0.35 was assumed, following others in the literature [15].

3. Member Characterization

To replicate the cell walls in the hexagonal honeycomb, special specimens were designed that approximate the ASTM D638 specimens in the grip section, but the gauge section is replaced with a slender member, shown in Figure 8, that has the exact thickness (0.032 inch) and process parameters (exactly two contours – see reference [1]) as those used in each of the cell walls in the hexagonal honeycomb.
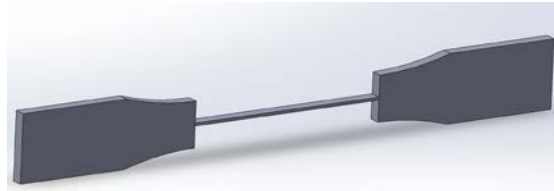
Figure 8. Specimen designed to have a thickness identical to the cell walls of the hexagonal honeycomb

Sixteen of these specimens were manufactured on the same machine (Fortus 400mc) used to make the honeycomb, and carefully removed from the build platform without using any solvent, to be consistent with the processing conditions used in manufacturing the honeycomb. Six of these specimens were damaged during the removal process on account of their very small thickness, requiring delicate handling. The ten surviving specimens were tested under tension on the Instron 8801 with a 50kN load cell, relying on crosshead displacement for the computation of strains, and load cell readings for stress. The specimens were pulled at a displacement rate of 5 mm/min.

The resulting stress-strain plots are shown in Figure 9. Failure strains vary for all samples, potentially on account of defects either during the printing process itself or specimen removal from the build sheet. With regard to the concern of this work, average elastic moduli was estimated at 285,972 psi. Conversion of the engineering stress-strain plots to true stress-strain plots, shown for a representative curve in Figure 10, generated a yield strength value of 4,855.3 psi and a tangent modulus of 6,317.1 psi associated with observed strain hardening. The yield point was estimated as the first point on the true stress-strain curve with zero-slope, in keeping with recommendations in the ASTM D638 standard [16]. Interestingly, while the modulus is lower than that quoted in the datasheet, the estimated yield strength is higher (the datasheet does not specify a tangent modulus). This may be attributable to dimensional variation as shown in Figure 3 – these were not explicitly corrected for, the assumption being made that the test specimen represents the honeycomb walls with regard to geometry and processing history. Table 1 summarizes these material properties from the two different sources.
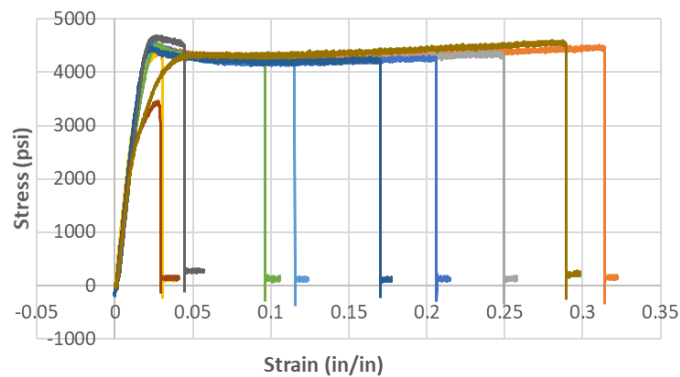
Figure 9. Engineering stress-strain plots from testing ten specimens under tension
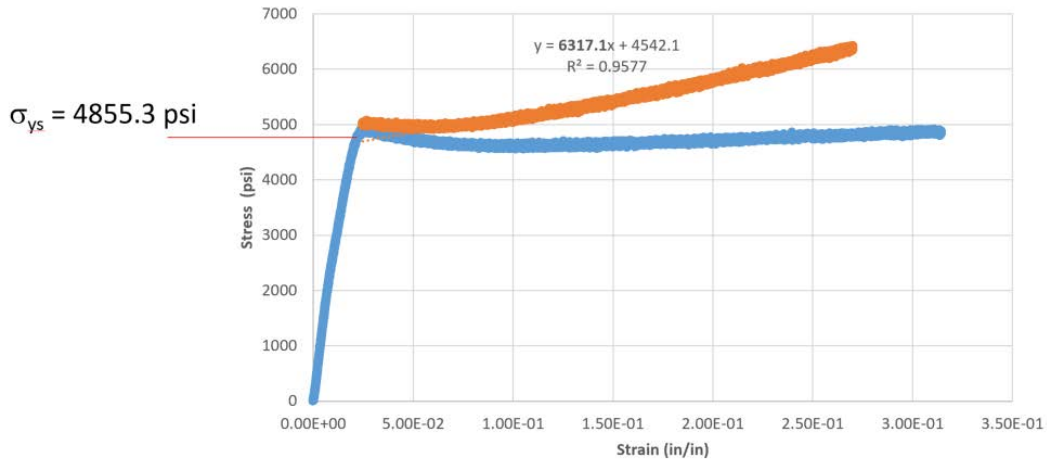
Figure 10. Representative curve from Figure 9, replotted as a True Stress-True Strain curve

Table 1. FDM ABS Material Properties Used in Models

	Young's Modulus E_s (psi)	Poisson's Ratio v_s	Yield Strength σ_{ys} (psi)	Tangent Modulus T_s (psi)
Bulk Property (Datasheet)	320,000	0.35	4,550	*Not Available*
Member Characterization	285,972	0.35	4,855	6317.1

Modeling Methods

Our goal with modeling is to predict the elastic and the initial plastic response of the honeycomb shown in Figure 7, based on the characterization data discussed in the previous section. There are two approaches we can take to develop these predictions: the analytical techniques developed by Gibson and Ashby [17] coupled with the use of homogenization techniques, treating the honeycomb as a block of solid material, or by using Finite Element Analysis (FEA). For each of these methods, we can use material property data from different sources. We discuss each of these methods below.

1. Homogenization Approach

The analytical methods developed by Gibson and Ashby [17] can be used for modeling both the elastic modulus and the yield stress of a regular honeycomb structure. Specifically, the in-plane effective elastic modulus for a hexagonal honeycomb under compression is given as:

$$E_1^* = E_2^* = \frac{4}{\sqrt{3}} E_s \left(\frac{t}{l}\right)^3 \frac{1}{1+(5.4+1.5\vartheta_s)(t/l)^2} \qquad (2)$$

where E_1^* and E_2^* represent the elastic modulus in the two in-plane directions (which are equal since the regular hexagonal honeycomb is a transversely isotropic structure), E_s and v_s are the

modulus and the Poisson's ratio of the material that makes up the honeycomb. t and l are geometry parameters corresponding to the thickness and length of the hexagonal honeycomb unit cell. Using this equation however tends to under-predict stiffness since it assumes the entire length l of the beam in the unit cell is contributing towards bending when in reality it is a smaller length that truly does so, as was described in a paper by Malek and Gibson that made a correction to the length calculation [18]. The revised calculation gives the reduced length l_b as:

$$l_b = l - \frac{t}{2\cos\theta} \tag{3}$$

where Θ is 30° for a regular hexagonal honeycomb. This result for l_b from equation 3 replaces l in equation 2.

Gibson and Ashby also developed expressions for failure stresses in honeycomb depending on the mode of failure (brittle vs plastic collapse) [17]. Careful observation of the failure mode in the honeycomb experiments conducted in this study show the clear formation of a plastic hinge as shown in Figure 11, followed by interfacial separation, the latter of which is driven by the dual contour layout of the process. Our interest for this work is in the initiation of plastic collapse, for which we may use the following equation derived by Gibson and Ashby for the plateau stress σ_{pl}^{*} honeycombs that exhibit such a failure mode:

$$\sigma_{pl}^{*} = \frac{2}{3}\left(\frac{t}{l_b}\right)^2 \sigma_{ys} \tag{4}$$

where σ_{ys} is the yield strength of the material.

To convert the stress and modulus equations into force-displacement diagrams that will enable a comparison to experimental data, we treat the honeycomb as a block of material with cross-sectional area and gauge length governed by the bounding box that the structure is contained by. The cross-section area is estimated by the depth of the honeycomb (b) multiplied by the width (w), the gauge length for purposes of strain calculation was taken as the height of the honeycomb (h). These values for the honeycomb used in this study are given in Table 2.
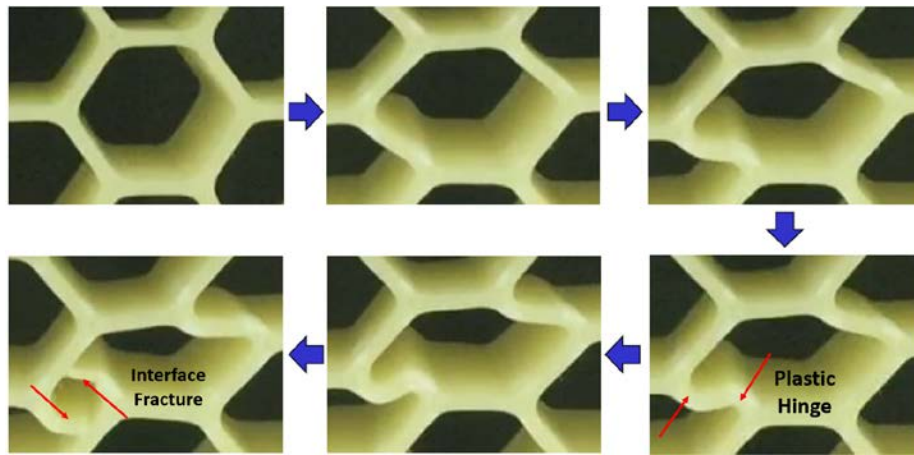
Figure 11. Close-up examination of deformation and failure mechanism of the honeycombs used in this study, clearly showing formation of a plastic hinge prior to interfacial failure

Table 2. Relevant dimensions of honeycomb used in this study [1]

Thickness (t)	Length (l)	Effective Length (l_b)	t/l_b
0.032 inch	0.18 inch	0.1615 inch	0.1981

b	w	h
1 inch	3.10 inches	3.15 inches

Substituting the values in Tables 1 and 2 into equations 2 and 4 allows for the estimation of the following relationships between load and displacement in the elastic regime (elastic stiffness) and the load at yield, listed in Table 3 for each of the two material assumptions (from the datasheet and from the member characterization).

Table 3. Elastic and Yield Load-displacement Estimates Based on Homogenization Approach

	Bulk Property (Datasheet)	Member Characterization
Elastic Stiffness (lbf/in)	4587.33	4099.52
Load at Yield (lbf)	369.02	393.76

To relate this to the experimental result in Figure 6, the elastic stiffness value is used to provide an estimate of the initial force-displacement response up to the load at yield, at which point perfect plasticity is assumed (no hardening or softening) to create the graph in Figure 12. Both datasets do a reasonable job of predicting the elastic response at low strains but do not replicate the plastic behavior adequately. The bulk property estimation performs better in the elastic regime, but is worse in the plastic regime.
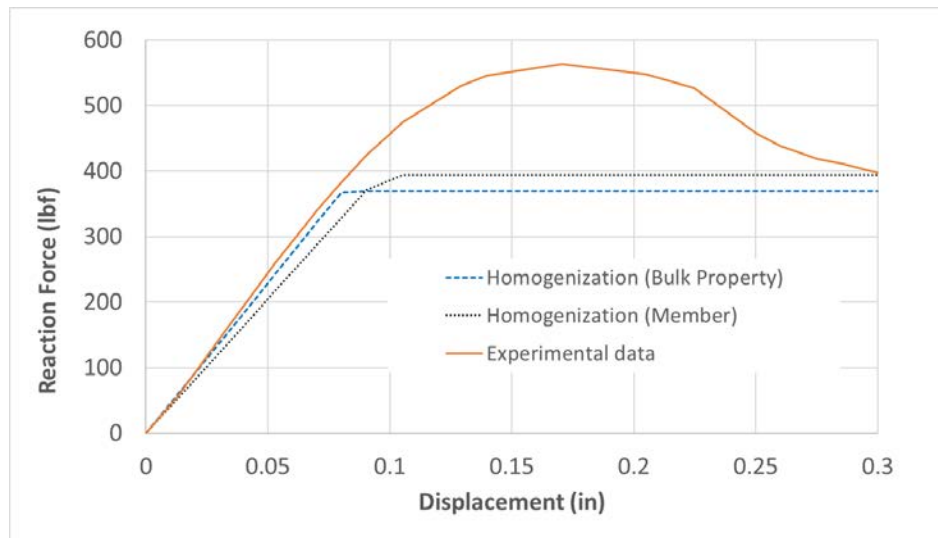
Figure 12. Comparison between experimental data and homogenization model using bulk property and member characterization estimations

2. FEA Approach

Using FEA we are able to explicitly model the honeycomb in its geometric detail, which we are unable to do with an analytical approach. The honeycomb CAD model was directly used

in ANSYS™ FEA software with one modification. Following our own observations and other published literature [19], it is known that fillets at the corners of honeycombs and lattices can significantly increase the stiffness of the cellular material. Data collected using blue-light scanning revealed an average fillet radius of 0.05 inches (shown for one specimen and corner in Figure 13). This corner was included in the CAD file for analysis to ensure greater accuracy in prediction of response of the honeycomb structure.
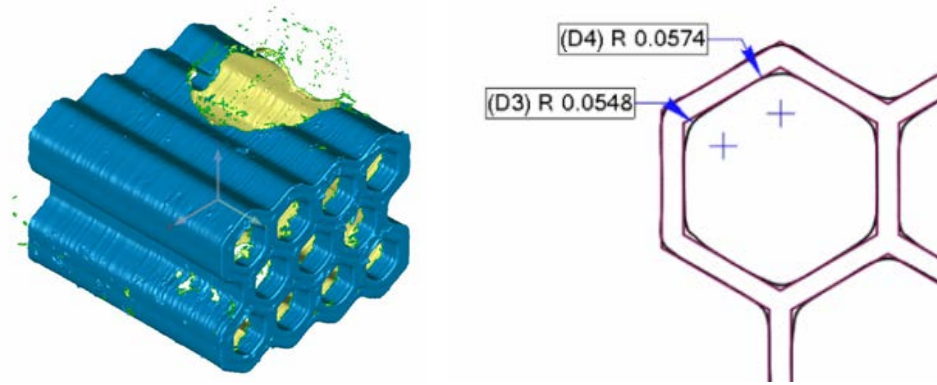
Figure 13. (left) Blue light scan of a honeycomb structure enabling (right) the measurement of corner radius. Results shown here are slightly higher than the average radius estimated for the hexagonal honeycomb at 0.05 inches (the speck on the scan is lost data associated with a marker)

The model was setup as a 2D plane strain problem, with frictional contacts applied at the top and bottom platens (friction coefficient of 0.15). The precise value of this coefficient was not experimentally estimated – this number was selected since it was at the low end for what would yield a converging solution without rigid body motion. Displacements were applied at one platen, the other was fixed and used for the measurement of reaction forces. The model was setup for both material models: bulk property and member level characterization, from table 1. Figure 14 demonstrates the setup, along with a close-up showing the mesh. Mesh refinement studies were conducted and once displacement results changed by less than 4%, further mesh refinement was ignored. Large deflection effects were included in the analysis.
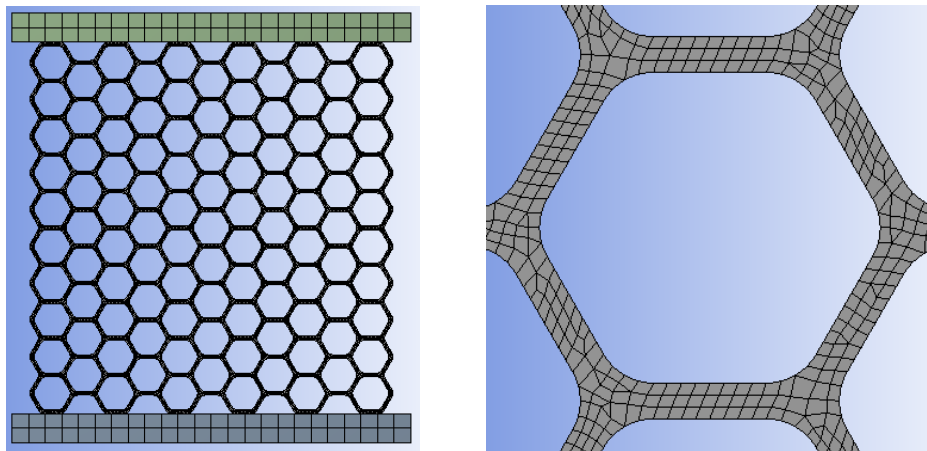
Figure 14. (left) 2D plane strain model with platens connected to honeycomb with frictional contacts and (right) close-up of an individual cell showing the mesh size as well as corner radius modeled after experimental measurements

Figure 15 shows results of the analysis, with equivalent plastic strains accumulating along two hinge points as observed experimentally and anticipated theoretically. While the precise location of the hinging within the honeycomb is not the same, the formation of a collapsing series of cells along a 30 degree line is consistent – indeed this was observed experimentally for all specimens tested [1]. The reaction force – displacement plots for both material models is shown in Figure 16, comparing against the experimental dataset – the plastic region is captured with greater detail with the FEA model, as compared to the analytical homogenization approach, as is to be expected due to the local and nonlinear nature of the deformation.

(a) (b)

(c) (d)
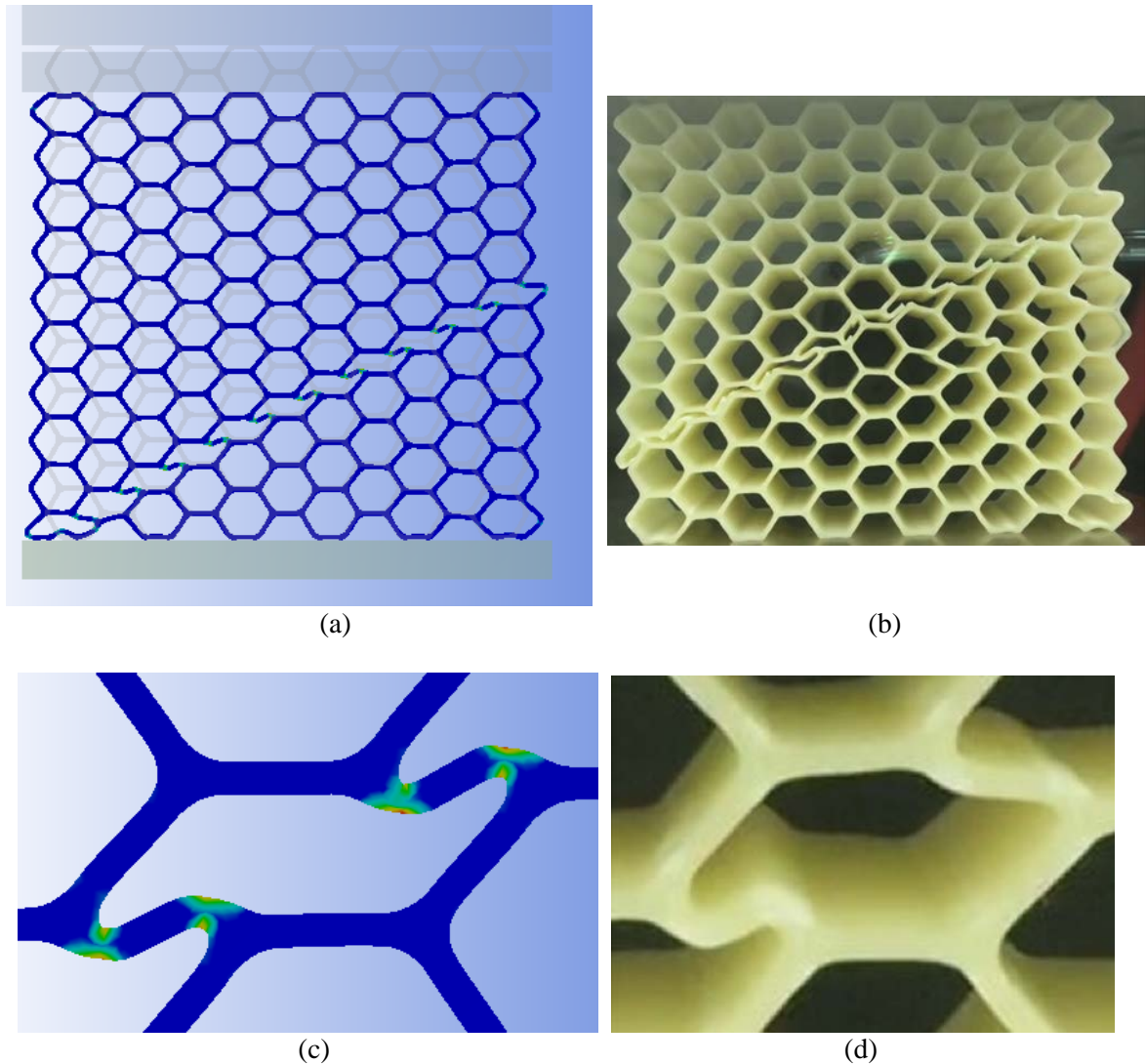
Figure 15. Equivalent plastic strain contour (a) showing localization of deformation consistent with experimental observations (b). Equivalent plastic strain contours (c) within a plastically deformed cell shows plastic hinging consistent with experimental observation (d) and with theory [17]
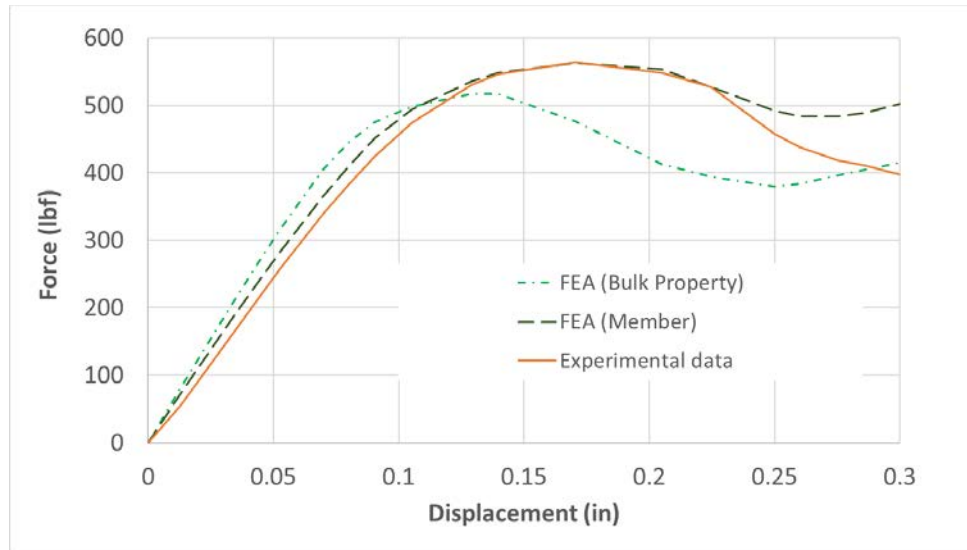
Figure 16. FEA model with two different material property assumptions compared against experimental result

Limitations of Study

This study has several limitations that limit its immediate applicability. We point these out and suggest further work needed to expand this work.

i. Sample size: Only one hexagonal honeycomb formed the basis of the experimental dataset. While it was part of the larger referenced study that looked at size effects [1], and fell within expected lines, it is by no means statistically significant. A larger sample size is needed to address this issue.

ii. Geometry, Process and Material Specificity: This work was conducted with the Fused Deposition Modeling process using ABS and for the hexagonal honeycomb structure only. For other combinations of process, material and geometry, findings may be different. Specifically, the formation of a plastic hinge is critical to the use of the analytical result as well as is likely a key reason why good agreement is obtained with an elastic-plastic material model (without accounting for fracture toughness, for example). Similar work needs to be conducted for different materials, geometries and processes to assess how these modeling methods hold up.

iii. Strain Rate Dependence: This work ignores the effects of strain rate dependence, which is known to be significant for plastics at ambient temperatures and for metals at high homologous temperatures particularly. Further, this may be exacerbated by the complex geometry and localization of strains in the structure, even if it is globally deformed at a seemingly quasi-static rate [20], [21]. More work is needed to assess the effect of strain rates on these modeling methods and the conclusions drawn below.

iv. 2D vs 3D Modeling: This work was conducted for the relatively straightforward 2D geometry of the honeycomb. The estimation of member data for a 3D lattice can be significantly more challenging due to orientation effects. Additionally, computational expense is very significant for the analysis of such a 3D structure. In this case, a blended approach that combines member modeling with homogenization maybe more appropriate.

Conclusions

In this work, we have compared two different approaches of modeling and two different characterization methods specifically for the Fused Deposition Modeling processing technology and for hexagonal honeycombs. While all methods do reasonably well in the elastic regime, modeling plastic behavior requires incorporation of geometry effects in FEA. To enable a meaningful *quantitative* comparison between the curves all plotted together in Figure 17, we applied a correlation coefficient comparing each dataset against the experimental baseline. The correlation coefficient is given as:

$$Correl\ (X,Y) = \frac{\sum(x-\bar{x})(y-\bar{y})}{\sqrt{\sum(x-\bar{x})^2 \sum(y-\bar{y})^2}} \qquad (5)$$

where *x* and *y* represent the two quantities being compared, and the barred quantities represent their respective averages. Using this correlation coefficient, we can now quantify how well representative each model is of the experimental dataset, and this is compiled for the four approaches in Table 4. This confirms our visual intuition, that the combination of a FEA modeling approach with material properties extracted from member level characterization most closely approximates the experimental data, with a correlation coefficient approaching 0.99.

It is reiterated that the above conclusion applies only to the process, material and structure studied in this work. More work is needed to ascertain how this methodology would perform for other processes and geometries, and how it would work in 3D cellular structures such as lattices.
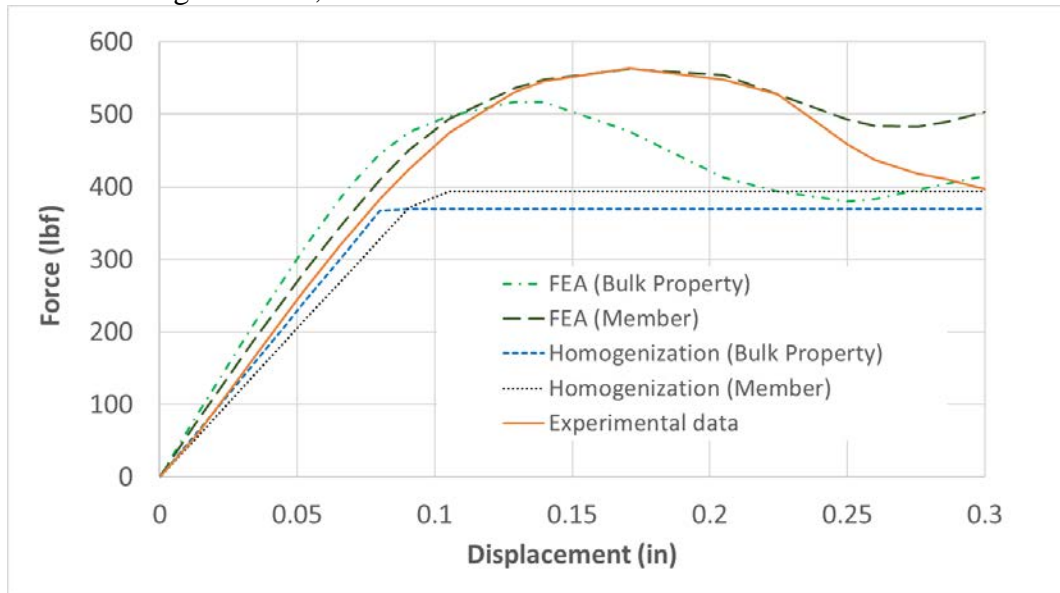
Figure 17. A comparison of all four methods and the experimental dataset, replotted on one graph

Table 4. Comparison of Correlation Coefficients for the Four Models against Experimental Data

Method	Homogenization (Bulk Property)	Homogenization (Member)	FEA (Bulk Property)	FEA (Member)
Correlation Coefficient	0.9595	0.9384	0.9210	0.9857

Acknowledgements

Disclaimer

References

[1]   T. Le, D. Bhate, J. M. Parsey, and K. H. Hsu, "Determination of a Shape and Size Independent Material Modulus for Honeycomb Structures in Additive Manufacturing," *Solid Free. Fabr. Symp.*, 2017.

[2]   L. Liu, P. Kamm, F. García-Moreno, J. Banhart, and D. Pasini, "Elastic and failure response of imperfect three-dimensional metallic lattices: the role of geometric defects induced by Selective Laser Melting," *J. Mech. Phys. Solids*, vol. 107, pp. 160–184, 2017.

[3]   C. Neff, N. Hopkinson, and N. B. Crane, "Selective Laser Sintering of Diamond Lattice Structures: Experimental Results and FEA Model Comparison," in *Solid Freeform Fabrication Symposium*, 2015.

[4]   M. Smith, Z. Guan, and W. J. Cantwell, "Finite element modelling of the compressive response of lattice structures manufactured using the selective laser melting technique," *Int. J. Mech. Sci.*, vol. 67, pp. 28–41, 2013.

[5]   C. Yan, L. Hao, A. Hussein, P. Young, and D. Raymont, "Advanced lightweight 316L stainless steel cellular lattice structures fabricated via selective laser melting," *Mater. Des.*, 2014.

[6]   P. Zhang *et al.*, "Efficient Design-Optimization of Variable-Density Hexagonal Cellular Structure by Additive Manufacturing: Theory and Validation," *J. Manuf. Sci. Eng.*, vol. 137, no. 2, p. 021004, 2015.

[7]   M. Mazur, M. Leary, S. Sun, M. Vcelka, D. Shidid, and M. Brandt, "Deformation and failure behaviour of Ti-6Al-4V lattice structures manufactured by selective laser melting (SLM)," *Int. J. Adv. Manuf. Technol.*, vol. 84, no. 5–8, pp. 1391–1411, 2016.

[8]   L. Cheng, P. Zhang, E. Biyikli, J. Bai, J. Robbins, and A. To, "Efficient design optimization of variable-density cellular structures for additive manufacturing: theory and experimental validation," *Rapid Prototyp. J.*, vol. 23, no. 4, pp. 660–677, 2017.

[9]   D. Bhate *et al.*, "A validated methodology for predicting the mechanical behavior of ULTEM-9085 honeycomb structures manufactured by fused deposition modeling," in

Solid Freeform Fabrication Symposium, 2016, pp. 2095–2106.

[10] S. Zhang, S. Dilip, L. Yang, H. Miyanaji, and B. Stucker, "Property Evaluation of Metal Cellular Strut Structures via Powder Bed Fusion AM."

[11] S. M. Ahmadi *et al.*, "Mechanical behavior of regular open-cell porous biomaterials made of diamond lattice unit cells," *J. Mech. Behav. Biomed. Mater.*, vol. 34, pp. 106–115, 2014.

[12] R. Gümrük, R. A. W. Mines, and S. Karadeniz, "Determination of Strain Rate Sensitivity of Micro-struts Manufactured Using the Selective Laser Melting Method," *J. Mater. Eng. Perform.*, vol. 27, no. 3, pp. 1016–1032, 2018.

[13] S. Tsopanos *et al.*, "The Influence of Processing Parameters on the Mechanical Properties of Selectively Laser Melted Stainless Steel Microlattice Structures," *J. Manuf. Sci. Eng.*, vol. 132, no. 4, p. 041011, 2010.

[14] Stratasys, "ABS-M30 Datasheet," 2017.

[15] J. Cantrell *et al.*, "Experimental Characterization of the Mechanical Properties of 3D Printed ABS and Polycarbonate Parts," *Rapid Prototyp. J.*, vol. 23, no. 4, pp. 811–824, 2017.

[16] ASTM International, *Standard test method for tensile properties of plastics*. pp. 1–17.

[17] L. J. Gibson and M. F. Ashby, *Cellular Solids: Structure and Properties*, 2nd ed. Cambridge Solid State Science Series, 1999.

[18] S. Malek and L. Gibson, "Effective elastic properties of periodic hexagonal honeycombs," *Mech. Mater.*, vol. 91, no. P1, pp. 226–240, 2015.

[19] J. B. Berger, H. N. G. Wadley, and R. M. McMeeking, "Mechanical metamaterials at the theoretical limit of isotropic elastic stiffness," *Nature*, vol. 543, no. 7646, pp. 533–537, 2017.

[20] D. Chan, X. Nie, D. Bhate, G. Subbarayan, and I. Dutta, "High strain rate behavior of Sn3.8Ag0.7Cu solder alloys and its influence on the fracture location within solder joints," in *Proceedings of the ASME InterPack Conference 2009, IPACK2009*, 2010, vol. 1.

[21] D. Bhate, D. Chan, G. Subbarayan, T. C. Chiu, V. Gupta, and D. R. Edwards, "Constitutive behavior of Sn3.8Ag0.7Cu and Sn1.0Ag0.5Cu alloys at creep and low strain rate regimes," *IEEE Trans. Components Packag. Technol.*, vol. 31, no. 3, 2008.